Eleventh International Conference on Computational Fluid Dynamics (ICCFD11), Maui, HI, July 11-15, 2022

ICCFD11-2022-4103

Simulating Paraffin Wax Droplets Using Mixed Finite Element Method

Darsh K. Nathawani[1] and Matthew G. Knepley[2]
Corresponding author: darshkir@buffalo.edu

[1]Computational and Data-enabled Science and Engineering, University at Buffalo, Buffalo, NY 14260, USA.
[2]Department of Computer Science and Engineering, University at Buffalo, Buffalo, NY 14260, USA.

Abstract: Paraffin wax is a prominent solid fuel for hybrid rockets. The atomization process of the paraffin wax fuel into he hybrid rocket combustion involves the droplets pinching off from the fuel surface. Therefore, droplet formation and pinch-off dynamics is analyzed using a one-dimensional axisymmetric approximation to understand droplet size distribution and pinch-off time. A mixed finite element formulation is used to solve the numerical problem. The computational algorithm uses adaptive mesh refinement to capture singularity and runs self-consistently to calculate droplet elongation. The code is verified using the Method of Manufactured Solution (MMS) and validated against laboratory experiments. Moreover, paraffin wax simulations are explored for varying inlet radius and it is found that the droplet size increases very slightly with the increasing inlet radius. Also, the pinch-off time increases up to a point where it starts to decrease as we increase the inlet radius. This behavior leads to a conjecture for the theoretical maximum radius that the droplet approaches as the inlet radius increases, which is a motivation for the future work.

Keywords: Droplet pinch-off dynamics, Mixed finite elements, Paraffin wax.

1 Introduction

Hybrid rockets uses a solid fuel and liquid oxidizer to produce the trust. Paraffin wax is a prominent candidate among high regression rate fuels for hybrid rocket engines [1]. As shown in the Fig. 1, the turbulent oxidizer blows over the top surface of the fuel grain. The fuel grain regresses partly due to direct evaporation and partly due to atomization [2]. The atomization of the paraffin wax, that begins by droplet formation and pinch-off, enables rapid burning and generates much more specific thrust than other fuels. Understanding pinch-off dynamics for paraffin wax, and in turn predicting of droplet sizes and pinch-off times, is crucial for designing and modeling hybrid rocket engines.

Surface tension is the chief factor that causes the breakup of a fluid thread in finite time. This breakup phenomenon is seen in many cases, like liquid bridges, breakup of a jet, droplet pinch-off, etc [3]. The particular case of a pendent drop has been explored in detail due to its relative simplicity. The gravitational force extends the droplet as it becomes heavier. The surface tension reduces the droplet radius from the middle to minimize the surface energy. Eventually the radius goes to zero and the droplet separates from the parent fluid column. The detailed analytical solutions for a pendent droplet before and after breakup was explained by Jens Eggers [4]. Furthermore, the pinch-off dynamics of a pendent droplet were explored experimentally [5, 6] and numerically [7, 8] using water and glycerol as example cases. Eggers and Dupont [7] introduced a one-dimensional approach to this problem using axisymmetric assumptions. They developed a finite difference model for simulating the pendent water droplet up to first pinch-off. However, they had to handle the domain length calculation explicitly using the tip velocity. Ambravaneshwaran et al. [8] extended

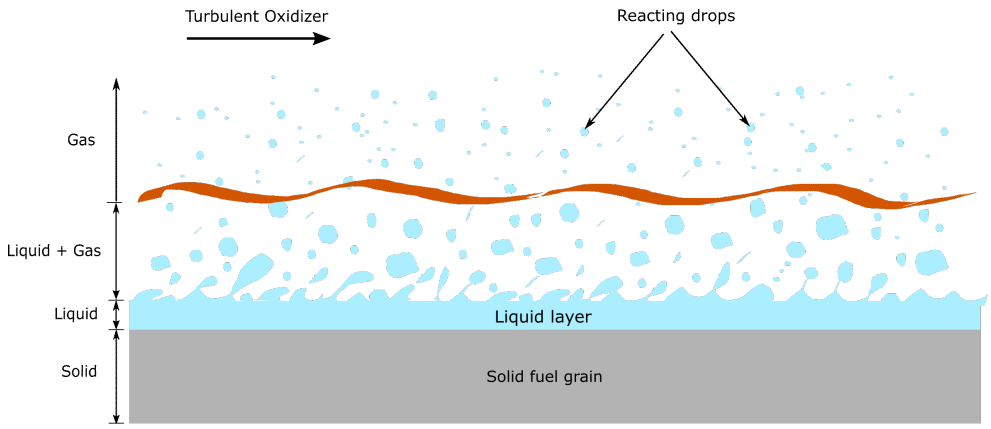

Figure 1: Schematic of a combustion chamber of hybrid rocket showing droplet pinch-off and atomization of the fuel.

the numerical study by developing a finite element approach. Moreover, they were able to explore the same problem using a two-dimensional domain and concluded that the one-dimensional approach provides very accurate results. However, they approach the length calculation using the volume constraint, which adds a dense row in the Jacobian matrix. Neither algorithm is available in open source code, nor in a parallel implementation.

In this study, we create a novel finite element model for gravity-driven droplet dynamics. Our implementation incorporates a self-consistent algorithm and adaptive mesh refinement. The domain length calculation is done using the tip velocity and the compared against volume constraint in a self-consistent iteration. We verify our model with the Method of Manufactured Solution (MMS), and then validate it against laboratory experiments on water and glycerol droplets.

2 Modeling approach

We consider one-dimensional axisymmetric fluid column described by the Navier-Stokes equations in cylindrical coordinates as treated by Eggers and Dupont [7]. The interface is tracked using an advection equation.

$$\frac{\partial u_r}{\partial t} + u_r\frac{\partial u_r}{\partial r} + u_z\frac{\partial u_r}{\partial z} = -\frac{1}{\rho}\frac{\partial p}{\partial r} + \nu\left(\frac{\partial^2 u_r}{\partial r^2} + \frac{\partial^2 u_r}{\partial z^2} + \frac{1}{r}\frac{\partial u_r}{\partial r} - \frac{u_r}{r^2}\right) \tag{1}$$

$$\frac{\partial u_z}{\partial t} + u_r\frac{\partial u_z}{\partial r} + u_z\frac{\partial u_z}{\partial z} = -\frac{1}{\rho}\frac{\partial p}{\partial z} + \nu\left(\frac{\partial^2 u_z}{\partial r^2} + \frac{\partial^2 u_z}{\partial z^2} + \frac{1}{r}\frac{\partial u_z}{\partial r}\right) - g \tag{2}$$

$$\frac{\partial h}{\partial t} + u_z\frac{\partial h}{\partial z} = u_r|_{r=h} \tag{3}$$

The above governing equations are simplified using the asymptotic expansion of the field variables. The radial shrinking is much faster than the elongation of the fluid column. Therefore, we expand the velocity (u_r, u_z) and pressure (p) using a Taylor series in 'r' which contains only even order terms due to the axisymmetry assumption. Also, the surface tension is coupled to the momentum equation using the force balance on the interface.

$$\hat{\mathbf{n}}\sigma\hat{\mathbf{n}} = -\gamma\left(\nabla\cdot\hat{\mathbf{n}}\right)$$
$$\hat{\mathbf{n}}\sigma\hat{\mathbf{t}} = 0$$

Here, σ is a stress tensor, $\hat{\mathbf{n}}$ is a unit outward normal, $\hat{\mathbf{t}}$ is a unit tangent, and $\nabla\cdot\hat{\mathbf{n}}$ is a mean curvature. The

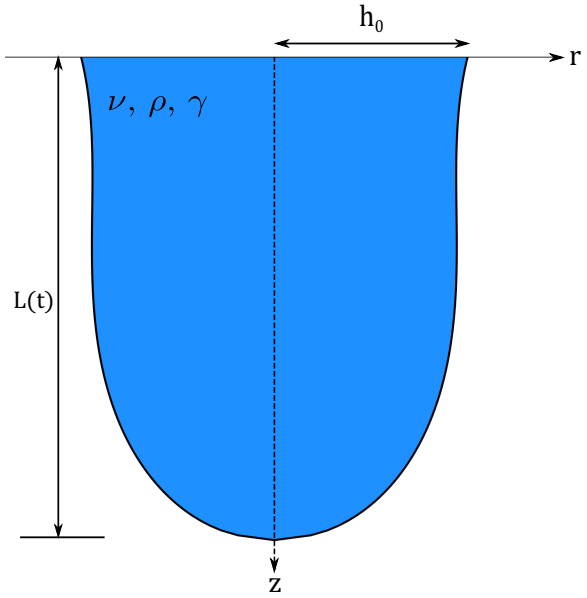

Figure 2: Schematic of a pendent droplet.

above force balance explains that the normal stress is balanced by the surface tension and the tangential stress is zero.

Using the force balance and the leading order terms in r from the expansion, we simplify the momentum equation. The advecting surface equation is already in leading order. Dropping the subscripts, the governing equations for one-dimensional axisymmetric fluid column is given by

$$\frac{\partial u}{\partial t} + u\frac{\partial u}{\partial z} + \frac{\gamma}{\rho}\frac{\partial(\nabla\cdot\hat{\mathbf{n}})}{\partial z} - \frac{3\nu}{h^2}\frac{\partial}{\partial z}\left(h^2\frac{\partial u}{\partial z}\right) - g = 0 \tag{4}$$

$$\frac{\partial h}{\partial t} + u\frac{\partial h}{\partial z} + \frac{h}{2}\frac{\partial u}{\partial z} = 0 \tag{5}$$

where, the mean curvature term $\nabla\cdot\hat{\mathbf{n}}$ is given by

$$\nabla\cdot\hat{\mathbf{n}} = \left[\frac{1}{h\left(1+\frac{\partial h}{\partial z}^2\right)^{1/2}} - \frac{\frac{\partial^2 h}{\partial z^2}}{\left(1+\frac{\partial h}{\partial z}^2\right)^{3/2}}\right]$$

Here, the curvature term is not approximated to the leading order because it has been shown that using the full curvature term better captures the singularities [4].

We use finite element discretization method for this problem. However, the system of Eq.(4- 5) has a third order derivative, which is difficult to handle using C^0 continuous elements. Therefore, we use mixed finite elements, augmented by a new variable (s) to simplify the curvature term. This will reduce the derivative order to second order. Using integration by parts, it can be approximated using C^0 elements. The weak

form using q, v, and w as test functions, is given by

$$\int_\Omega q\left[\frac{\partial u}{\partial t}+u\frac{\partial u}{\partial z}+\frac{\gamma}{\rho}\frac{\partial(\nabla\cdot\hat{\mathbf{n}})}{\partial z}-\frac{3\nu}{h^2}\frac{\partial}{\partial z}\left(h^2\frac{\partial u}{\partial z}\right)-g\right]d\Omega=0 \tag{6}$$

$$\int_\Omega v\left[\frac{\partial h}{\partial t}+u\frac{\partial h}{\partial z}+\frac{1}{2}h\frac{\partial u}{\partial z}\right]d\Omega=0 \tag{7}$$

$$\int_\Omega w\left[s-\frac{\partial h}{\partial z}\right]d\Omega=0 \tag{8}$$

where, the curvature term is

$$\nabla\cdot\hat{\mathbf{n}}=\left[\frac{1}{h\left(1+s^2\right)^{1/2}}-\frac{\frac{\partial s}{\partial z}}{\left(1+s^2\right)^{3/2}}\right]$$

Initially, the velocity is zero and the curvature profile is a hemisphere as that minimizes surface energy. The inlet radius h_0 is fixed depending on the nozzle radius and the inflow velocity u_0 is constant. The radius at the tip of the droplet, at length $L(t)$, is zero. The set of Eq. (6)-(8) are then solved using a continuous Galerkin formulation subject to the following constraints.

Initial conditions:

$$\begin{aligned}
&h=\sqrt{h_0^2-z^2}\\
&s=-\frac{z}{\sqrt{h_0^2-z^2}}\ \text{for}\ (0\le z<L_0),\qquad s|_{L_0}=-C\\
&u=0
\end{aligned}$$

where, C is a large negative number. In our implementation, we use -10. However, the code was tested with larger values and results were unchanged.

Boundary conditions:

$z=0$	$h=h_0$	$u=u_0$
$z=L(t)$	$h=0$	$u=\frac{dL}{dt}$

Figure 2 shows a schematic of a pendent droplet in cylindrical coordinates. The length of the droplet varies with time, so that the computational domain is moving. However, the length is implicitly involved in the system and can be calculated using either (1) the tip velocity or (2) the volume constraint. The first approach is simple, we calculate the velocity as a part of the solution and use that for length calculation. However, there is a chance that we undershoot or overshoot the total volume due to discretization error. On the other hand, the second approach ensures the volume conservation but adds a dense row to the Jacobian matrix. We can combine these two approaches to keep the calculation simple while still ensuring volume conservation.

Another subtlety in solving the problem on a moving domain is that the changing mesh coordinates invalidate the solution representation. When the mesh is changed every time-step using the length evaluation, the solution has to be projected onto the deformed mesh. This can be achieved using Galerkin projection. We simply apply new dual basis on the old basis to get the interpolated coefficient values on the new mesh points [9]. The length calculation, moving the mesh using the length and projecting the solution onto the new mesh can be done in a self-consistent iteration. This algorithm is explained in detail in [10].

Finally, we use adaptive mesh refinement as we seek droplet evolution approaching the pinch-off. Low viscosity fluids, such as water, are difficult to simulate due to their highly convective nature. Therefore, we use Streamline Upwinding (SU) scheme in our numerical model. The SU scheme regularizes the added diffusion, where the regularization parameter depends on the element size [11]. Hence, the added diffusion decreases as we refine the mesh adaptively.

3 Results

A verification study is crucial for any computational model in order to obviate any coding errors. We verify our code using the Method of Manufactured Solution (MMS) [12]. The details of the mesh convergence study are explained in [10]. Similarly, the validation study is important to confirm the underlying physics that is being simulated. The computational model is validated with previous experimental work by Zhang and Basaran [6]. Figure 3 shows the evolution of non-dimensional droplet length in time away from the pinch-off for water and 85% glycerol solution. The plot shows an excellent agreement of the numerical simulation results with the experimental data. The water droplet quickly approaches the pinch-off, causing less elongation of the neck due to very low viscosity. Compared to that, the glycerol takes more time to approach the pinch-off, resulting in longer neck caused by the damping effect of high viscosity. Droplet profiles are attached to the corresponding solution points to visualize the evolution. The water droplet develops a smaller neck compared to the glycerol droplet. This is due to the higher viscosity of the glycerol solution.

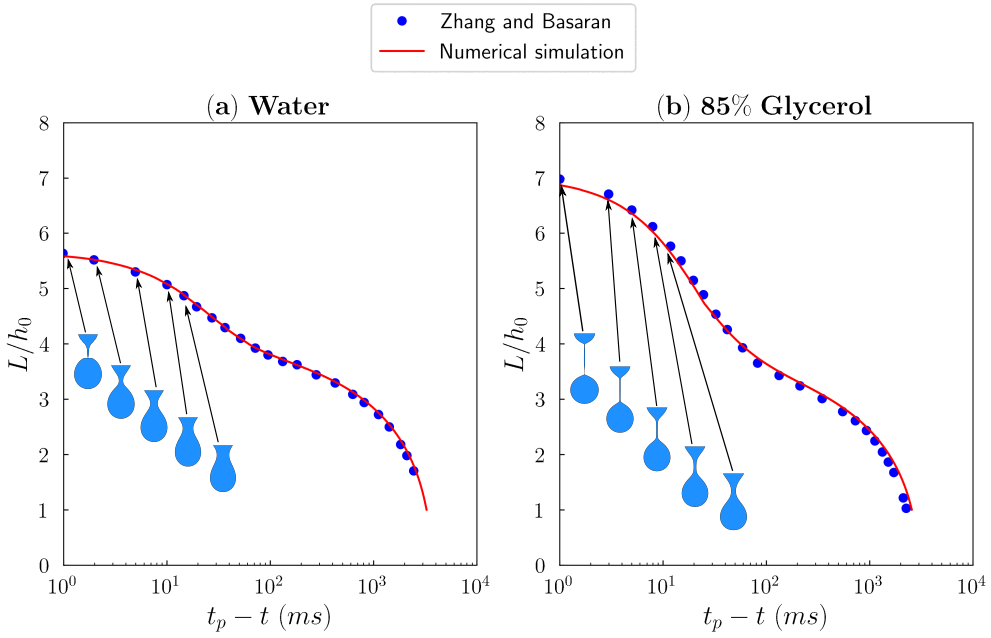

Figure 3: Evolution of non-dimensional length in time approaching the pinch-off for (a) water and (b) 85% glycerol. The inlet radius $h_0 = 0.0016$ m and inflow rate = 1 mL/min.

3.1 Paraffin wax

The exploration of paraffin wax droplet sizes and pinch-off time is useful in predicting the atomization volume and regression rate of the fuel in a hybrid rocket engine. In this section, we explore the volume distribution and the pinch-off time of paraffin wax. The material properties data is given in [10]. We use 1 mL/min volume flow rate, which provides the inlet velocity for the given inlet radius. Figure 4 shows the non-dimensional length of the droplet at the time of pinch-off for different inlet radii of the liquid paraffin wax. The non-dimensional length decreases as the inlet radius increases. For smaller radius, the gravitational force elongates the fluid column once the fluid mass is enough. Then the surface tension can start acting against the gravitational force. For smaller inlet radius case, the top region of the fluid starts to regain the hemisphere shape. As the radius increases, the top region profile becomes more flat. The smaller radius droplet has less fluid compared to larger radius. Hence, the surface tension force dominates the gravitational force for smaller radius droplet, making it hemispherical at the top. Moreover, the droplet shape transits from oval to spherical as the inlet radius increases. However, the pinch-off droplet sizes are not changing with the same order as the inlet radius. Specifically, the droplet sizes look very similar for the last two inlet

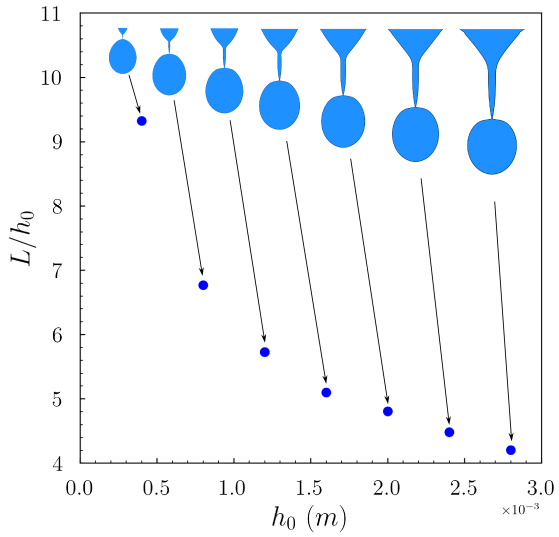

Figure 4: Non-dimensional length for various inlet radii of the paraffin wax droplet.

radii. We postulate that the pinched off droplets may have a maximum radius that they approach as we increase the inlet radius. More simulations and/or analytical solution are needed to confirm this conjecture.

The analysis of pinch-off droplet volume can be useful to understand the volume of wax that is leaving the parent fluid. Figure 5 shows the pinch-off time as we increase the inlet radius. The smaller inlet radius droplets pinch off faster compared to large inlet radius. The figure also shows the volume of the pinched off droplet per unit time. Initially, the volume per unit time shows slightly decreasing trend because the pinch-off time increases. However, as the pinched off droplet gets larger with increasing inlet radius, the increase in volume surpasses the increase in pinch-off time; ultimately increasing volume per unit time.

The total time for break up to occur depends on the inlet radius (h_0), density (ρ), and the surface tension (γ), if neglecting the viscosity [13]. The equation for pinch-off time can be derived for first order

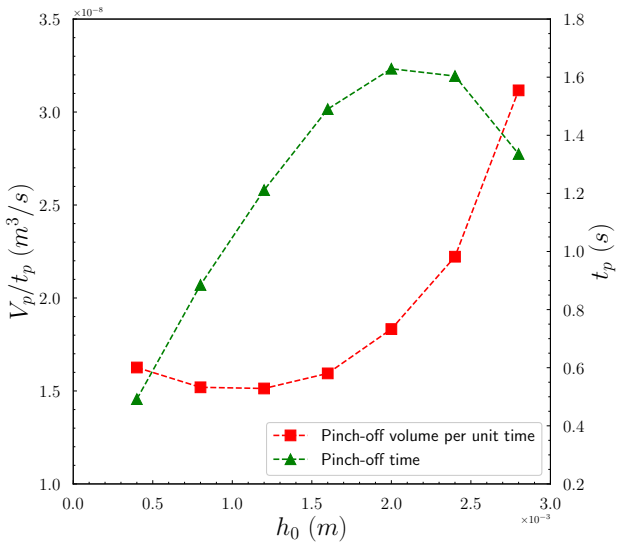

Figure 5: Pinch-off volume per unit time and pinch-off time for varying inlet radius.

approximation, where the viscosity does not play a role.

$$t_p = \left(\frac{\rho h_0^3}{\gamma}\right)^{\frac{1}{2}} \tag{9}$$

However, the pinch-off time increases up to a point where it stagnates and then goes down. This trend is different than the approximation given in Eq. 9. Higher order analytical investigation is required to confirm this behavior.

4 Conclusion and Future Work

A one-dimensional model is reliably accurate to simulate axisymmetric droplet formation. The present computational model is verified using MMS and validated against experimental data. The numerical results show excellent agreement with the experiments. The paraffin wax droplets are simulated to analyze the pinch-off volume and pinch-off time for a range of initial radii. For smaller inlet radius, the pinch-off volume per unit time shows increasing trend with increasing inlet radius. The pinch-off time increases with the increase in the inlet radius but turns around at some point and starts decreasing.

In future work, we expect to analyze the decrease in pinch-off time using more simulations. Moreover, we can explore the analytical solution to provide some insights into the maximum droplet size that can be achieved for a given fluid. Also, we plan to expand this model to incorporate shear-driven droplet formation in a background flow. This more closely matches the process of atomization in a hybrid rocket engine, and impacts both the pinch-off time and droplet volume. We propose to maximize the pinch-off volume per unit time to achieve maximum fuel regression.

References

[1] M. Karabeyoglu and B. J. Cantwell, "Combustion of liquefying hybrid propellants: Part 2, stability of liquid films," *Journal of Propulsion and Power*, vol. 18, no. 3, pp. 621–630, 2002.

[2] M. Karabeyoglu, D. Altman, and B. J. Cantwell, "Combustion of liquefying hybrid propellants: Part 1, general theory," *Journal of Propulsion and Power*, vol. 18, no. 3, pp. 610–620, 2002.

[3] J. Eggers, "Nonlinear dynamics and breakup of free-surface flows," *Reviews of modern physics*, vol. 69, no. 3, p. 865, 1997.

[4] J. Eggers, "Theory of drop formation," *Physics of Fluids*, vol. 7, no. 5, pp. 941–953, 1995.

[5] X. Shi, M. P. Brenner, and S. R. Nagel, "A cascade of structure in a drop falling from a faucet," *Science*, vol. 265, no. 5169, pp. 219–222, 1994.

[6] X. Zhang and O. A. Basaran, "An experimental study of dynamics of drop formation," *Physics of fluids*, vol. 7, no. 6, pp. 1184–1203, 1995.

[7] J. Eggers and T. F. Dupont, "Drop formation in a one-dimensional approximation of the navier–stokes equation," *Journal of fluid mechanics*, vol. 262, pp. 205–221, 1994.

[8] B. Ambravaneswaran, E. D. Wilkes, and O. A. Basaran, "Drop formation from a capillary tube: Comparison of one-dimensional and two-dimensional analyses and occurrence of satellite drops," *Physics of Fluids*, vol. 14, no. 8, pp. 2606–2621, 2002.

[9] P. Farrell and J. Maddison, "Conservative interpolation between volume meshes by local galerkin projection," *Computer Methods in Applied Mechanics and Engineering*, vol. 200, no. 1-4, pp. 89–100, 2011.

[10] D. K. Nathawani and M. G. Knepley, "Droplet formation simulation using mixed finite elements," *Physics of Fluids*, vol. 34, no. 6, p. 064105, 2022.

[11] J. Donea and A. Huerta, *Finite element methods for flow problems*. John Wiley & Sons, 2003.

[12] P. J. Roache, "Code verification by the method of manufactured solutions," *J. Fluids Eng.*, vol. 124, no. 1, pp. 4–10, 2002.

[13] J. Eggers and E. Villermaux, "Physics of liquid jets," *Reports on progress in physics*, vol. 71, no. 3, p. 036601, 2008.